Original Article

Rapid liver tissue characterization using simultaneous multi-relaxation-time imaging: a comparative study with conventional magnetic resonance imaging

Yuanqiu Jiang[1,2#^], Peiyuan Yin[3#], Yishuang Wang[1,2], Meining Chen[4], Longlin Yin[1,2]

[1]Department of Radiology, Sichuan Academy of Medical Sciences & Sichuan Provincial People's Hospital, University of Electronic Science and Technology of China, Chengdu, China; [2]Institute of Radiation Medicine, Sichuan Academy of Medical Sciences & Sichuan Provincial People's Hospital, University of Electronic Science and Technology of China, Chengdu, China; [3]Department of Radiology, Affiliation Hospital of Southwest Medical University, Luzhou, China; [4]MR Research Collaboration, Siemens Healthineers Ltd., Chengdu, China

Contributions: (I) Conception and design: Y Jiang, P Yin; (II) Administrative support: L Yin; (III) Provision of study materials or patients: Y Jiang, P Yin, Y Wang; (IV) Collection and assembly of data: Y Jiang, Y Wang, M Chen; (V) Data analysis and interpretation: Y Jiang, L Yin; (VI) Manuscript writing: All authors; (VII) Final approval of manuscript: All authors.

[#]These authors contributed equally to this work as co-first authors.

Correspondence to: Longlin Yin, MD. Department of Radiology, Sichuan Academy of Medical Sciences & Sichuan Provincial People's Hospital, University of Electronic Science and Technology of China, No. 32 West Second Section 1st Ring Rd., Chengdu 610072, China; Institute of Radiation Medicine, Sichuan Provincial People's Hospital, Chengdu, China. Email: yinlonglin@163.com.

Background: With the increasing need for accurate liver disease diagnostics, non-invasive imaging techniques with rapid and precise quantitative measurements need to be established. This study introduced and validated the application of simultaneous multi-relaxation-time imaging (TXI) for the quantitative assessment of liver tissue by simultaneously acquiring proton density fat fraction (PDFF), lateral relaxation rate (R2*), and longitudinal relaxation time (T1) maps. It aimed to compare the accuracy and consistency of TXI with established quantitative magnetic resonance imaging (MRI) techniques, such as three-dimensional variable flip angle (VFA) T1 mapping, and multi-point quantitative Dixon (qDixon), in healthy volunteers and patients diagnosed with non-alcoholic fatty liver disease (NAFLD).

Methods: A prospective cohort of 35 healthy volunteers (mean age: 52±13 years, 21 women) and nine NAFLD patients (mean age: 48±13 years, 6 women) underwent liver MRI using TXI, VFA T1 mapping, and qDixon sequences. Intraclass correlation coefficients (ICCs) and Bland-Altman plots were used to assess inter-observer agreement and measurement consistency. Paired *T*-tests and Pearson correlation coefficients were used to compare the TXI measurements with those from conventional MRI techniques. Differences between the healthy volunteers and NAFLD patients were evaluated using the independent sample *T*-test.

Results: The ICCs for the TXI-derived T1, R2*, and PDFF in healthy volunteers were 0.985 [95% confidence interval (CI): 0.971–0.993], 0.999 (95% CI: 0.998–1.000), and 0.995 (95% CI: 0.990–0.997), respectively, indicating excellent agreement. The regression analysis revealed strong correlations between the TXI and reference MRI measurements for the T1 (R^2=0.895), R2* (R^2=0.984), and PDFF (R^2=0.894) values with no significant differences (P=0.713, 0.090, and 0.072, respectively). Statistically significant differences were observed in the R2* (P=0.045) and PDFF (P<0.001) values between the NAFLD patients and healthy volunteers, but no significant difference was observed in the T1 values (P=0.965). Multiparametric imaging showed that TXI provides comprehensive liver tissue characterization, consistent with conventional MRI techniques.

^ ORCID: 0009-0002-6745-8844.

Conclusions: TXI offers a rapid and reliable method for the simultaneous acquisition of T1, R2*, and PDFF maps, and has high consistency with established quantitative MRI techniques. This approach has significant potential for non-invasive liver tissue characterization in clinical settings, particularly in the diagnosis and monitoring of conditions such as NAFLD.

Keywords: Magnetic resonance imaging (MRI); non-alcoholic fatty liver disease (NAFLD); liver fibrosis

Submitted Aug 25, 2024. Accepted for publication Mar 04, 2025. Published online Apr 28, 2025.
doi:10.21037/qims-24-1786
View this article at: https://dx.doi.org/10.21037/qims-24-1786

Introduction

In recent years, non-alcoholic fatty liver disease (NAFLD) has become one of the most common chronic liver diseases worldwide, and has a global prevalence of more than 30% (1). NAFLD may progress to end-stage liver disease such as liver fibrosis and cirrhosis (2). Early treatment can effectively block the progression of NAFLD and can even reverse the process of liver fibrosis (3). In addition, approximately one-third of NAFLD patients have iron overload, and elevated liver iron content may result in an increased risk of liver fibrosis and liver cancer (4). Thus, the early and accurate assessment of pathological changes and their severity in NAFLD patients, and an understanding of the complex interactions among liver fat content, iron concentration, and fibrosis are essential for the management of NAFLD.

Currently, liver biopsy is the gold standard for the diagnosis and staging of NAFLD (5). However, liver biopsy has some limitations such as invasiveness, sampling error, and a risk of complications (6). Thus, a non-invasive, quantitative, and reproducible method needs to be established to accurately assess NAFLD in clinical settings.

With the development of magnetic resonance imaging (MRI) technology, quantitative MRI technology has become an effective and non-invasive method for evaluating the characteristics of liver tissue (7). Magnetic resonance elastography (MRE) is a widely used method for measuring liver cirrhosis and liver fibrosis. The diagnostic accuracy of MRE is high; however, it requires additional hardware and setup time, although recent advancements allow for faster acquisition with multiple slices obtained in a single breath-hold (8). In recent years, the use of longitudinal relaxation time (T1) mapping to quantitatively assess liver fibrosis and inflammation, particularly the three-dimensional variable flip angle (VFA) T1 sequence, has gained increasing attention. The T1 value is closely related to the severity of liver fibrosis. It is significantly correlated with MRE measurement results and histopathology, and thus could potentially serve as an alternative biomarker for the quantitative assessment and longitudinal monitoring of liver fibrosis (9-12). The multi-point quantitative Dixon (qDixon) sequence can simultaneously obtain liver lateral relaxation rate (R2*) and the proton density fat fraction (PDFF), which has been widely used in clinical practice. Studies have confirmed that R2* values are highly correlated with liver iron content as determined by biopsy results (R^2=0.95–0.98), and are even superior to liver biopsy in the continuous monitoring of changes in liver iron content (13-15). Thus, R2* values are a reliable tool for the non-invasive quantitative assessment of liver iron overload. The PDFF is widely recognized as an MRI quantitative imaging biomarker for the non-invasive assessment of hepatic steatosis. The PDFF, which is derived from qDixon techniques, exhibits high diagnostic accuracy and sensitivity to small changes in fat content. Currently, it stands as an accurate, standardized, and objective indicator for the non-invasive measurement of liver tissue fat content (16-19). However, these multiparametric images are typically acquired by independent scans during different breath-holding processes, which can lead to patient fatigue. Additionally, this approach has a number of drawbacks, such as the potential misalignment of multiparametric images due to variations in respiratory movement and imaging parameters between subjects (20).

Several methods have been developed to acquire hepatic parametric maps. For example, high-dimensional model-guided deep dictionary learning has recently been developed to accelerate free-breathing four-dimensional whole-liver water-fat MRI (21). The simultaneous water-fat separation and T1 mapping of the whole-liver sequence simultaneously achieves water-fat separation and T1 mapping of the liver under free-breathing conditions (22). Additionally, multitask multi-echo MRI is used to quantify

T1, PDFF, and R2* values during free-breathing (23). These methods address the critical challenges of balancing motion robustness, acquisition speed, and multiparametric accuracy in hepatic MRI to varying extents, while advancing the clinical utility of quantitative liver imaging.

Simultaneous multi-relaxation-time imaging (TXI) has recently been used in the liver and spine, with preliminary studies confirming its repeatability and accuracy in the quantitative diagnosis of disc degeneration (24,25). TXI allows for the simultaneous acquisition of liver T1, R2*, and PDFF values during a single breath-hold, avoiding the problems associated with misalignment in multiparameter imaging. However, the application of TXI technology in quantitative liver studies is still in its early stages, and its accuracy is unknown. Thus, this study aimed to verify the accuracy of TXI in liver quantitative evaluation by comparing TXI with VFA T1 localization and qDixon sequences. We present this article in accordance with the STROBE reporting checklist (available at https://qims.amegroups.com/article/view/10.21037/qims-24-1786/rc).

Methods

Theory

TXI is an advanced MRI technique designed to simultaneously quantify multiple parameters, including the PDFF, R2*, and T1 values, in a single imaging protocol. Unlike conventional methods that require separate acquisitions for different relaxation parameters, TXI integrates a multi-echo gradient-echo (ME-GRE) sequence with a VFA approach to acquire the PDFF, R2*, and T1 maps. However, rather than acquiring all data in a single breath-hold, TXI performs two separate ME-GRE scans, each acquired in an independent breath-hold, one at a lower flip angle (typically 4°), and one at a higher flip angle (typically 10°). This dual-acquisition strategy allows for the simultaneous quantification of multiple tissue properties, while ensuring signal accuracy for T1 mapping.

In each breath-hold, multiple gradient echoes are acquired to facilitate PDFF and R2* quantification. The multi-echo signal model used in TXI can be represented as:

$$S_n = \left(M_w + M_f \sum_{p=1}^{m} \alpha_p e^{i2\pi\Delta f_p t_n n} \right) e^{i2\pi\psi t_n} e^{-R_2^* t_n} \quad [1]$$

where S_n represents the signal at the nth echo time (TE); M_w and M_f are the magnitudes of the water and fat signals, respectively; α_p denotes the relative contributions of the individual fat peaks; and m is the number of fat peaks, when $\sum_{p=1}^{m}=1$ it represents the total fat peak. Different values of m can be selected for different parts of adipose tissue (26,27). According to the nine-peak fat model proposed by Hamilton *et al.* (27), the chemical shifts (δ) and relative contribution percentages are as follows: 5.29 ppm (3.70%), 5.19 ppm (1.00%), 4.20 ppm (3.90%), 2.75 ppm (0.60%), 2.24 ppm (5.80%), 2.02 ppm (6.20%), 1.60 ppm (5.80%), 1.30 ppm (64.20%), and 0.90 ppm (8.80%). In addition, Δf_p represents the chemical shifts of each fat peak relative to the water proton, and ψ represents the inhomogeneity of the B0 field.

The multi-echo signals collected at different TEs are critical for the separation of water and fat signals, a process that is central to TXI. By analyzing the phase differences induced by the chemical shift between water and fat, TXI uses a qDixon-based approach to separate the water and fat signals. This separation is essential for calculating the PDFF, which is determined by dividing the fat signal magnitude M_f by the total signal magnitude $M_w + M_f$.

The R2* parameter, which reflects the rate of signal decay due to magnetic field inhomogeneities and tissue-specific relaxation properties, is obtained by analyzing how the signal intensity decreases across the different TEs (28). The decay is modeled as an exponential function of TE, with the decay rate directly proportional to R2*. To quantify R2*, a logarithmic transformation of the signal intensity is performed, converting the exponential decay into a linear relationship. The slope of the linear fit to the log-transformed data is the negative of the R2* value, allowing for the generation of a R2* map that details the spatial distribution of transverse relaxation rates in the tissue.

The T1 relaxation time is quantified using a VFA approach based on the method described by Fram *et al.* (29). This method solves a linearized steady-state gradient-echo signal equation using two different flip angles, ensuring accurate and efficient T1 estimation. The signal intensity at each flip angle can be described by the following equation:

$$S(FA') = \frac{M_0 \sin(FA')\left(1 - e^{-\frac{TR}{T1}}\right)}{1 - \cos(FA') \cdot e^{-\frac{TR}{T1}}} \quad [2]$$

where M_0 is the equilibrium magnetization, TR is the repetition time, and *FA'* is the actual flip angle, which may differ from the nominal value due to B1 field inhomogeneities. As T1 estimation requires measuring signal intensities at two different flip angles, TXI uses

two separate breath-hold acquisitions, ensuring consistent acquisition parameters, while allowing for the precise estimation of T1 values. B1 inhomogeneity is accounted for through an additional B1 mapping scan, which further improves the accuracy of the T1 quantification.

Study participants

The study was conducted in accordance with the Declaration of Helsinki and its subsequent amendments. The study was approved by the Institutional Review Board of Sichuan Academy of Medical Sciences & Sichuan Provincial People's Hospital, University of Electronic Science and Technology of China (No. 2023-550), and written informed consent was obtained from all participants before MRI. Healthy volunteers (n=40) and NAFLD patients (n=10) were enrolled in the study. All the participants underwent routine MRI and liver TXI examinations between December 2023 and March 2024. To be eligible for inclusion in the study, the healthy volunteers had to meet the following inclusion criteria: (I) be aged 18 to 75 years; (II) have no history of liver-related diseases (e.g., fatty liver, hepatitis, cirrhosis, or hepatocellular carcinoma); (III) have a body mass index (BMI) of 30 kg/m^2 or less. To be eligible for inclusion in the study, the patients had to meet the following inclusion criteria: (I) have histopathologically confirmed NAFLD; and (II) be aged 18 to 75 years. Participants in both groups were excluded from the study if they met any of the following exclusion criteria: (I) had contraindications to MRI examination or an inability to complete the MRI examination; (II) had other acute diseases or critical illnesses; and/or (III) had poor quality images. Three healthy volunteers with incidental fatty liver disease, two healthy volunteers, and one patient were excluded from the study due to severe breathing artifacts. Thus, ultimately, 35 healthy volunteers and 9 patients were included in the image analysis.

Imaging acquisition

Liver MRI scanning was performed using a 3.0T MRI scanner (Magnetom Vida, Siemens Healthineers, Erlangen, Germany). The participants were instructed to fast for at least 4 hours before the examination. All the participants underwent total liver TXI, VFA T1 mapping, and qDixon sequence scanning. For each participant, the localization for the TXI, VFA T1 mapping, and qDixon sequences was consistent. The TXI acquisition used a ME-GRE sequence, which included multiple echoes collected at the same TE for different flip angles (4° and 10°), ensuring uniformity in timing across acquisitions. Additionally, a separate B1 mapping scan was performed to correct B1 inhomogeneities. The scan parameters for each sequence are detailed in *Table 1*.

Imaging reconstruction and analysis

The image reconstruction and quantitative mappings of T1, R2*, and the PDFF were performed on all the TXI data using an in-house postprocessing software based on MatLab (R2018b, Mathworks, Inc., Natick, MA, USA) and Python ver.3.5 (Python Software Foundation, Delaware, USA). The outputs from the VFA T1 mapping and qDixon sequences were obtained directly from the workstation (Syngo via, Siemens Healthineers). The quantitative liver maps generated from TXI were labeled as TXI_T1, TXI_R2*, and TXI_PDFF mapping. Results from the VFA T1 mapping sequence were labeled as VFA_T1 mapping, while those from the qDixon sequence were labeled as Q_R2* and Q_PDFF mapping.

Two radiologists, with five and 30 years of experience in abdominal MRI, respectively, manually delineated a circular region of interest (ROI) of approximately 200–300 mm^2 on three slices of the right lobe of the liver (above, at, and below the hepatic hilum). The ROI placement included as much liver parenchyma as possible, while excluding large blood vessels, liver edges, and artifacts. For the TXI quantitative imaging, the ROIs were first delineated on the TXI_R2* mapping and then directly copied to the TXI_T1 and TXI_PDFF mappings to calculate the corresponding T1, R2, and PDFF values, which were then averaged across all the ROIs. For the qDixon imaging, the ROIs were plotted on the Q_R2* mapping and subsequently copied to the Q_PDFF and VFA_T1 maps to calculate the mean R2*, PDFF, and T1 values. The positioning of these ROIs was consistent with those used in the TXI imaging (*Figure 1*). All delineations and parameter calculations were performed manually using 3D Slicer ver. 5.2.1 (Slicer Community, Brigham and Women's Hospital, Boston, MA, USA). The measurements of the two radiologists were averaged for further analysis.

Statistical analysis

SPSS software ver.26.0 (IBM Corporation, Armonk, NY, USA) and MedCalc ver.22.01 (Medcalc software Ltd., Ostend, Belgium) were used for the statistical analysis. The

Table 1 Imaging parameters for TXI, VFA, qDixon, and B1 mapping sequences using 3.0 T MRI

Parameters	TXI	VFA	qDixon	B1 mapping
Coil	18-channel body array	18-channel body array	18-channel body array	18-channel body array
FOV (mm)	336×380	380×380	309×380	310×380
Matrix size	156×224	120×160	62×128	31×64
Slice thickness (mm)	4	4	4	8
No. of slices	52	52	52	18
Sequence dimensionality	3D	3D	3D	2D
Parallel imaging method	CAIPIRINHA	CAIPIRINHA	CAIPIRINHA	–
Acceleration factor	4	3	4	–
Phase encoding	2	1	2	–
Slice encoding	2	2	2	–
Phase partial Fourier	–	7/8	–	–
Phase resolution (%)	79	75	60	60
Slice resolution (%)	50	50	50	64
Flip angle (degrees)	4 and 10	3 and 15	4	8
TR (ms)	11.00	5.00	9.00	5,050.00
TE (ms)				
No. of echoes	6	1	6	1
First echo	1.07	2.20	1.05	1.83
Echo spacing	1.72	–	1.41	–
Acquisition time (s)	19	16	8	10

2D, two-dimensional; 3D, three-dimensional; CAIPIRINHA, controlled aliasing in parallel imaging results in higher acceleration; FOV, field of view; MRI, magnetic resonance imaging; qDixon, quantitative Dixon; TE, echo time; TR, repetition time; TXI, multi-relaxation-time imaging; VFA, variable flip angle.

T-test was employed for the normally distributed data, while non-parametric tests were employed for the non-normally distributed data. Descriptive statistics were used for the participant characteristics. For the healthy volunteers, Bland-Altman plots and intraclass correlation coefficients (ICCs) were used to assess the consistency of measurements between the TXI observers. A paired *T*-test was used to evaluate the differences between the T1, R2*, and PDFF values obtained using the TXI technique and those obtained using the reference quantitative MRI. Pearson correlation coefficients were used to evaluate the correlations between the two groups. The correlation values were categorized as follows: 0–0.19: very poor; 0.20–0.49: poor; 0.50–0.69: moderate; 0.70–0.89: strong; 0.90–1.00: excellent (30). An independent sample *T*-test was used to compare the results of the healthy volunteers and patients. For all the statistical tests, a P value <0.05 indicated a statistically significant difference.

Results

A total of 35 healthy volunteers (mean age: 52±13 years; age range: 24–72 years; 21 women, 14 men; average BMI: 22.8±2.6 kg/m^2; BMI range, 19.2–29.3 kg/m^2; average abdominal circumference: 79.3±7.8 cm; abdominal circumference range, 63.1–93.5 cm) and nine NAFLD patients (mean age: 48±13 years; age range, 32–69 years; 6 women, 3 men; average BMI: 25.0±2.0 kg/m^2; BMI range, 22.6–28.8 kg/m^2; average abdominal circumference: 86.1±7.0 cm; abdominal circumference range, 72.8–93.3 cm) were included in this study. All the data were confirmed to follow a normal distribution.

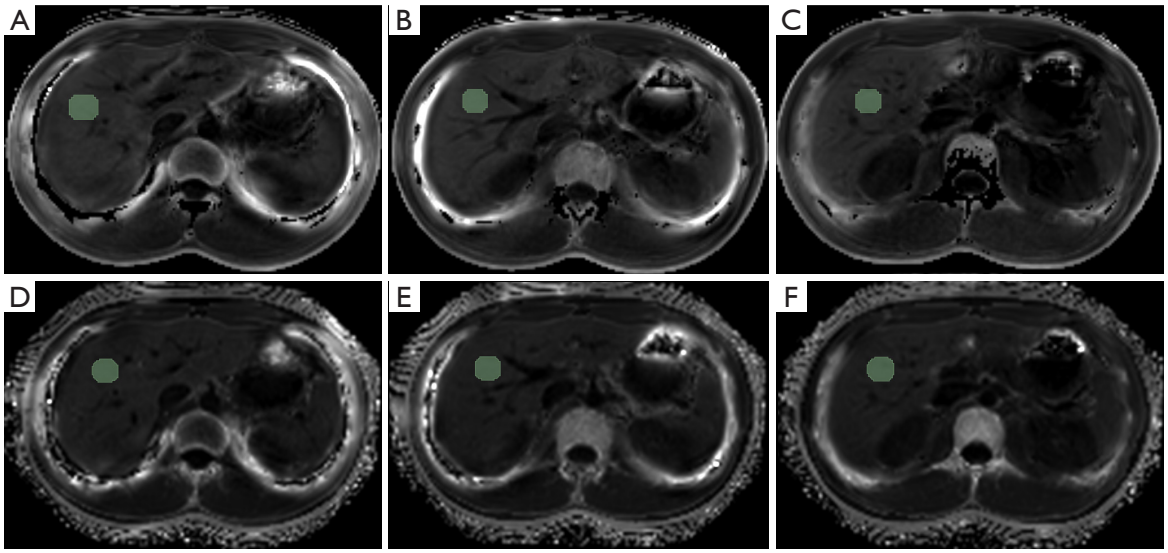

Figure 1 Schematic diagram of manually delineated ROIs for each parametric map. The green circles in (A-C) represent the ROI at the level above, level, and level below the hepatic portal in the TXI_R2* image, respectively. Similarly, the green circles in (D-F) represent the ROI at the level above, level, and level below the portal in the Q_R2* image, respectively. ROI, region of interest; TXI, multi-relaxation-time imaging.

In the clinical healthy volunteers, the TXI measurements yielded the following T1 values: mean: 889.1 ms, median: 898.4 ms, minimum: 716.8 ms, and maximum: 963.7 ms. While the R2* values were as follows: mean: 45.6 s^{-1}, median: 44.1 s^{-1}, minimum: 27.1 s^{-1}, and maximum: 67.4 s^{-1}. The PDFF values were as follows: mean: 2.6%, median: 2.7%, minimum: 1.5%, and maximum: 3.9%. The Bland-Altman analysis (*Figure 2*) showed the consistency of the TXI-derived T1, R2*, and PDFF measurements, and the ICC values between the two observers were 0.985 [95% confidence interval (CI): 0.971–0.993], 0.999 (95% CI: 0.998–1.000), and 0.995 (95% CI: 0.990–0.997), respectively. These high ICC values indicated excellent agreement across all parameters.

The regression analysis (*Figure 3*) of the TXI measurements and reference quantitative MRI measurements in the healthy volunteers showed strong correlations for the T1 (R^2=0.895, P=0.713), R2* (R^2=0.984, P=0.090), and PDFF (R^2=0.894, P=0.072). No statistically significant differences were observed between the TXI and reference measurements for any parameter, confirming the validity of the TXI method. *Figure 4* provides multiparametric TXI images of the liver of a representative healthy volunteer, which showed strong alignment with the reference quantitative MRI images.

In the patient cohort, the TXI-measured T1 values were as follows: mean: 920.0 ms, median: 870.0 ms, minimum: 734.2 ms, and maximum: 1219.7 ms. While the R2* values were as follows: mean: 55.0 s^{-1}, median: 54.6 s^{-1}, minimum: 28.0 s^{-1}, and maximum 75.8 s^{-1}. Notably, the PDFF values of the patients were high (mean: 8.2%; median: 8.7%, minimum: 2.4%, and maximum: 15.8%), much higher than healthy subjects.

Boxplots illustrating the T1, R2*, and PDFF values obtained from the TXI, VFA, and qDixon sequences in both the healthy volunteers and patients are shown in *Figure 5*. While there was no statistically significant difference in the T1 values between the two groups (P=0.965), the differences in the R2* (P=0.045) and PDFF (P<0.001) values were statistically significant, indicating that these parameters are sensitive to pathological changes. *Figure 6* provides a multiparametric image of a patient diagnosed with NAFLD, where elevated PDFF levels were detected using both the qDixon and TXI methods.

Discussion

With the global epidemic of chronic liver disease, an accurate, rapid, and safe method urgently needs to be established to determine the type and extent of chronic liver disease. As a non-invasive diagnostic tool, quantitative MRI can evaluate liver fibrosis, inflammation, iron overload, and steatosis using T1, R2*, and PDFF measurements, and has

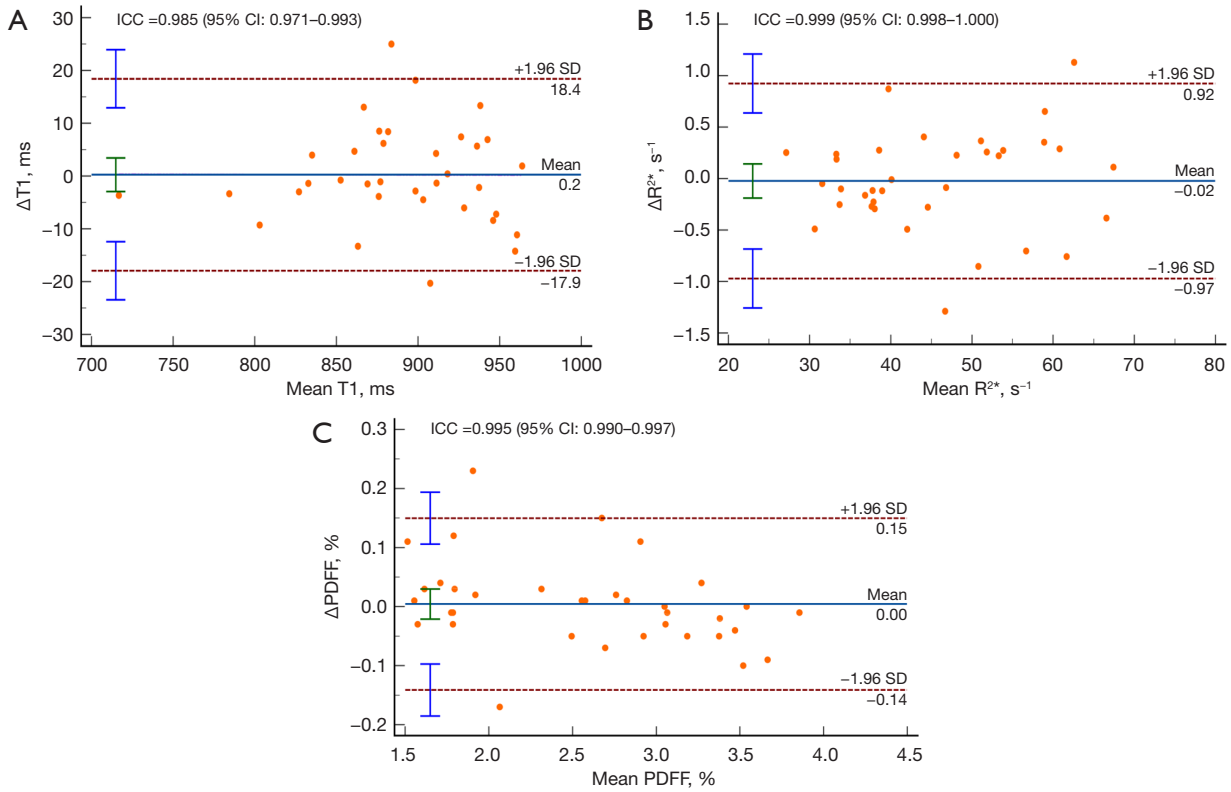

Figure 2 Bland-Altman analysis of liver TXI measurements in healthy volunteers by two independent observers. (A-C) Bland-Altman analyses and ICCs in TXI_T1, TXI_R2*, and TXI_PDFF for two observers, with ICCs of 0.985 (95% CI: 0.971–0.993), 0.999 (95% CI: 0.998–1.000), and 0.995 (95% CI: 0.990–0.997), respectively. CI, confidence interval; ICC, intraclass correlation coefficient; PDFF, proton density fat fraction; SD, standard deviation; TXI, multi-relaxation-time imaging.

been widely used in clinical practice. This study used the TXI imaging method to perform whole-liver T1, R2*, and the PDFF mapping in 19 seconds. In addition, additional B1 mapping was used to internally correct the inhomogeneity and stability of B1. All the parameters were measured in a single scan, eliminating the need for re-alignment that is often required when using multiple imaging methods.

qDixon is a well-established technique in the MRI system for quantifying the PDFF and R2*, and is known for its excellent reproducibility and clinical applicability (31). It has been shown to have high accuracy in the quantitative assessment of hepatic steatosis and iron deposition, can accurately stage severity, and even outperforms liver biopsy in the longitudinal assessment of disease changes (16-19). The T1 value obtained from the VFA T1 sequence is highly correlated with liver biopsy and MRE measurements, and has shown low bias, excellent reproducibility, and consistency across multiple vendors (32).

In this study, we found that the T1, PDFF, and R2* values measured using the TXI method were highly correlated with those obtained from VFA and qDixon in healthy volunteers (R^2 values of 0.895, 0.984, and 0.894, respectively). No significant differences were observed between the methods (P values of 0.713, 0.090, and 0.072, respectively). Previously, studies have reported that the T1, R2, and PDFF values of healthy liver tissue at 3.0T are approximately 948 ms, 51.8 s^{-1}, and 2.1%, respectively (23,33,34). In our study, the TXI-measured values in the healthy volunteers were 889.1±46.3 ms for T1, 45.6±8.7 s^{-1} for R2*, and 2.6%±0.6% for the PDFF. These values are comparable to those reported in the literature, indicating that the TXI-derived measurements align well with previously established data. Additionally, this study enrolled nine patients, and the T1, R2*, and PDFF values were calculated using the TXI method. In comparisons between the healthy volunteers and patients, no statistically significant differences in the T1 values were observed. This may be due to the limited sample size and the potential

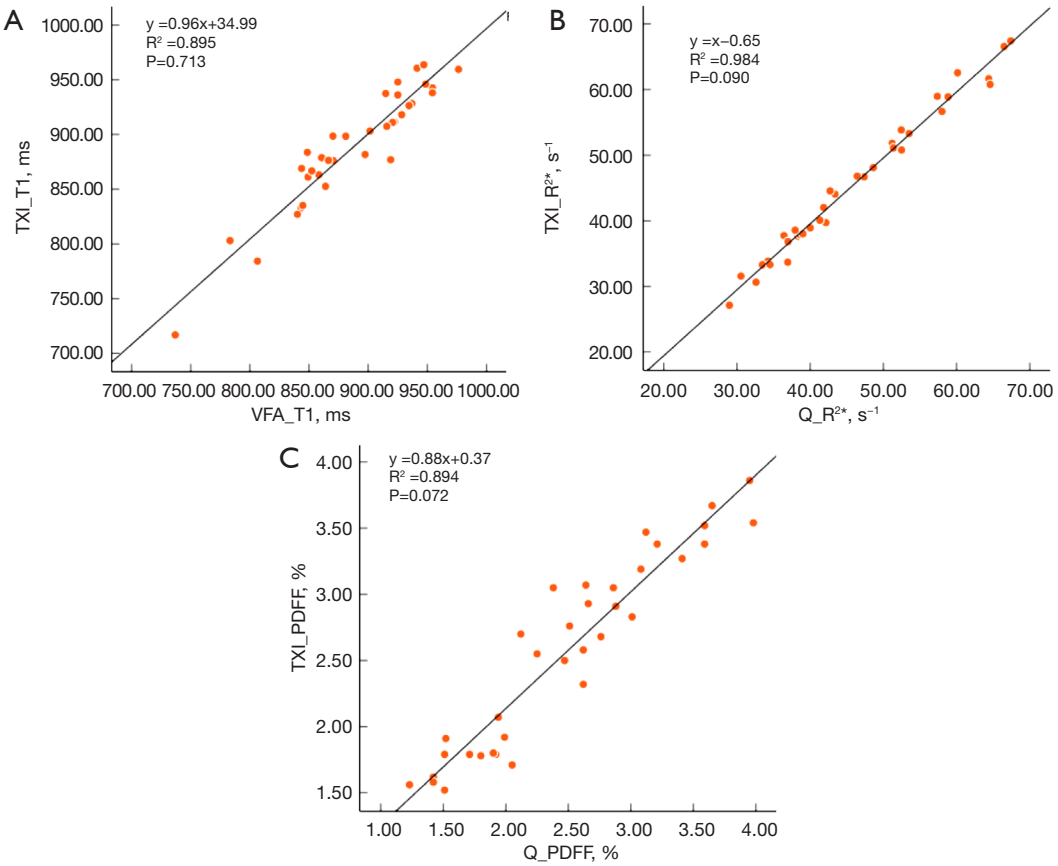

Figure 3 The correlation of the TXI with the VFA and qDixon measurements in the liver. The regression analysis comparing TXI with reference quantitative MRI showed good agreement between the T1 (A), R2* (B), and PDFF (C) values in the clinically healthy volunteers, with R^2 values of 0.895, 0.984, and 0.894, respectively. MRI, magnetic resonance imaging; PDFF, proton density fat fraction; qDixon, quantitative Dixon; R^2, Pearson correlation coefficients; TXI, multi-relaxation-time imaging; VFA, variable flip angle.

heterogeneity of liver diseases, which could also explain the presence of outliers in *Figure 5A*. Future studies should include a larger cohort of patients with liver diseases to validate these findings.

Reeder *et al.* proposed the iterative decomposition of water and fat with echo asymmetry and least-squares estimation (IDEAL), an improved water-fat separation technique based on Dixon's concept, which incorporates multiple fat subpeaks and allows flexible TEs to enhance the signal-to-noise ratio (35). However, the IDEAL assumes that only water, fat, and B0 inhomogeneity affect the signal, and neglects the effect of R2* decay. As a result, it performs poorly in tissues with high iron deposition, where R2* significantly attenuates the signal. To address this, Yu *et al.* introduced the T2*-IDEAL method, which incorporates R2* estimation into the water-fat separation process, improving the accuracy of fat quantification and enabling the simultaneous assessment of hepatic steatosis and iron overload (36). Despite these improvements, the IDEAL remains sensitive to phase errors, particularly when fat content is low (<20%), leading to PDFF estimation inaccuracies (37,38). To address this issue, modulus-based reconstruction methods use the Levenberg-Marquardt (LM) least-squares algorithm to eliminate B0 inhomogeneity effects. This approach refines R2* estimation and improves PDFF quantification, but it requires an initial water-fat estimate, and performs best in regions with large water-fat differences. In areas with minimal water-fat contrast, modulus-based reconstruction often suffers from poor signal-to-noise ratio (38).

To optimize PDFF and R2* estimation, we adopted a hybrid reconstruction method. First, the T2*-IDEAL algorithm generates an initial water-fat separation while accounting for R2* effects. This preliminary result is then used

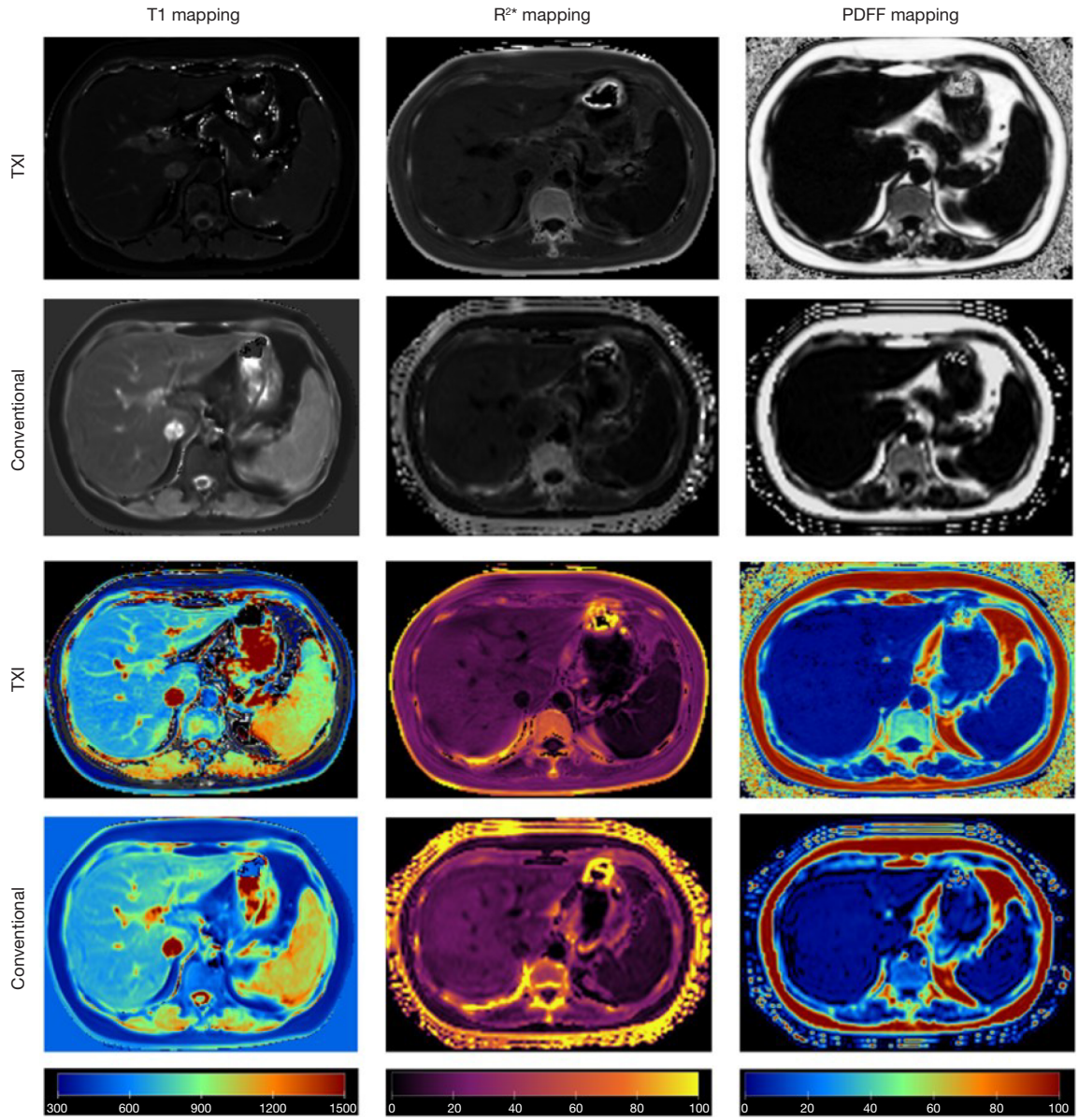

Figure 4 Original images of TXI and conventional MRI sequences (top two rows) are presented alongside their corresponding false color representations (bottom two rows) for a 24-year-old healthy male. The mean T1, R2*, and PDFF values measured by TXI were 946 ms, 32 s^{-1}, and 1.6%, respectively, and those measured by reference quantitative MRI were 948 ms, 31 s^{-1}, and 1.4%, respectively. MRI, magnetic resonance imaging; PDFF, proton density fat fraction; TXI, multi-relaxation-time imaging.

as an input for LM modulus fitting, which iteratively refines the water-fat quantification and R2* values. By integrating the strengths of both approaches, this method improves accuracy and robustness in hepatic fat and iron quantification.

TXI eliminates the need for cardiac gating, which is required in the modified look-locker inversion recovery (MOLLI) sequence for T1 mapping. MOLLI relies on electrocardiogram triggering and multiple cardiac cycles for accurate T1 estimation, making it more complex and less suitable for non-cardiac applications such as liver imaging (39). Conversely, TXI allows for the simultaneous acquisition of T1, R2*, and PDFF maps in a single scan, enabling comprehensive liver characterization, while maintaining efficiency and accuracy. Additionally, a

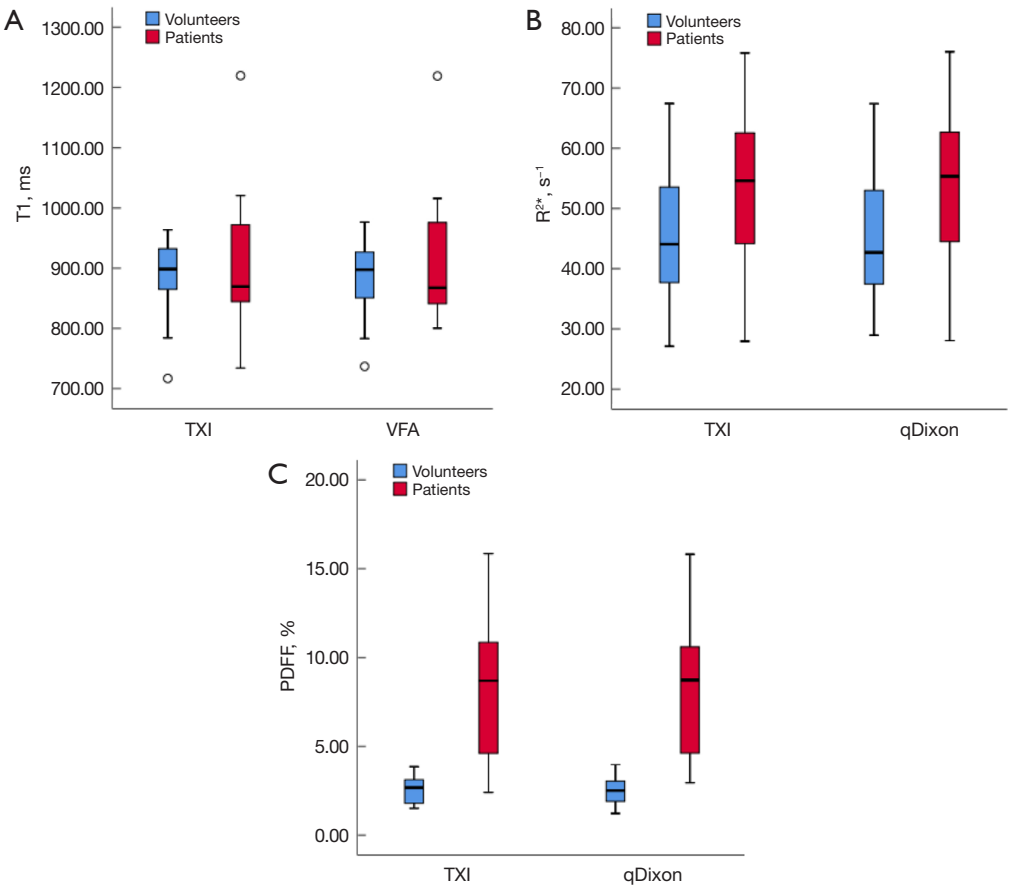

Figure 5 Box plots of TXI, VFA, and qDixon derived T1 (A), R2* (B), and PDFF (C) values for healthy volunteers and patients. In each box, the center marker represents the median, and the bottom and top edges represent the 25th and 75th percentiles, respectively, while the end of the line represents the maximum and minimum values, respectively. qDixon, multi-point quantitative Dixon; PDFF, proton density fat fraction; TXI, multi-relaxation-time imaging; VFA, variable flip angle.

key limitation of conventional VFA T1 mapping is its sensitivity to B1 inhomogeneity, which can lead to T1 underestimation by up to 30% at 3T (40). This variability affects measurement accuracy and reproducibility, particularly in abdominal imaging. To address this issue, a separate low-resolution B1+ map was acquired in this study to improve spatial uniformity and ensure more reliable T1 quantification (41).

This study had several limitations. First, while TXI integrates multiple quantitative MRI parameters into a single acquisition, it ends up with only one less breath hold compared to capturing PDFF/R2* and T1 maps separately. While this improves efficiency, the overall reduction in patient effort may be modest, and further advancements in motion compensation or accelerated imaging techniques may reduce breath-holding frequency/duration and improve work efficiency. Second, this study was conducted *in vivo* without phantom validation using reference T1 and PDFF values. As a result, the absolute accuracy of the TXI measurements could not be fully established. Future studies should include phantom experiments to confirm the reliability of TXI-derived parameters. Third, our study was limited by a small sample size, particularly in the patient cohort. A larger cohort would improve the statistical power and generalizability of our findings. Future studies with an expanded sample size, including patients with a wider range of liver pathologies, need to be conducted to further validate the clinical utility of TXI.

Conclusions

The liver TXI technique is a rapid and promising non-

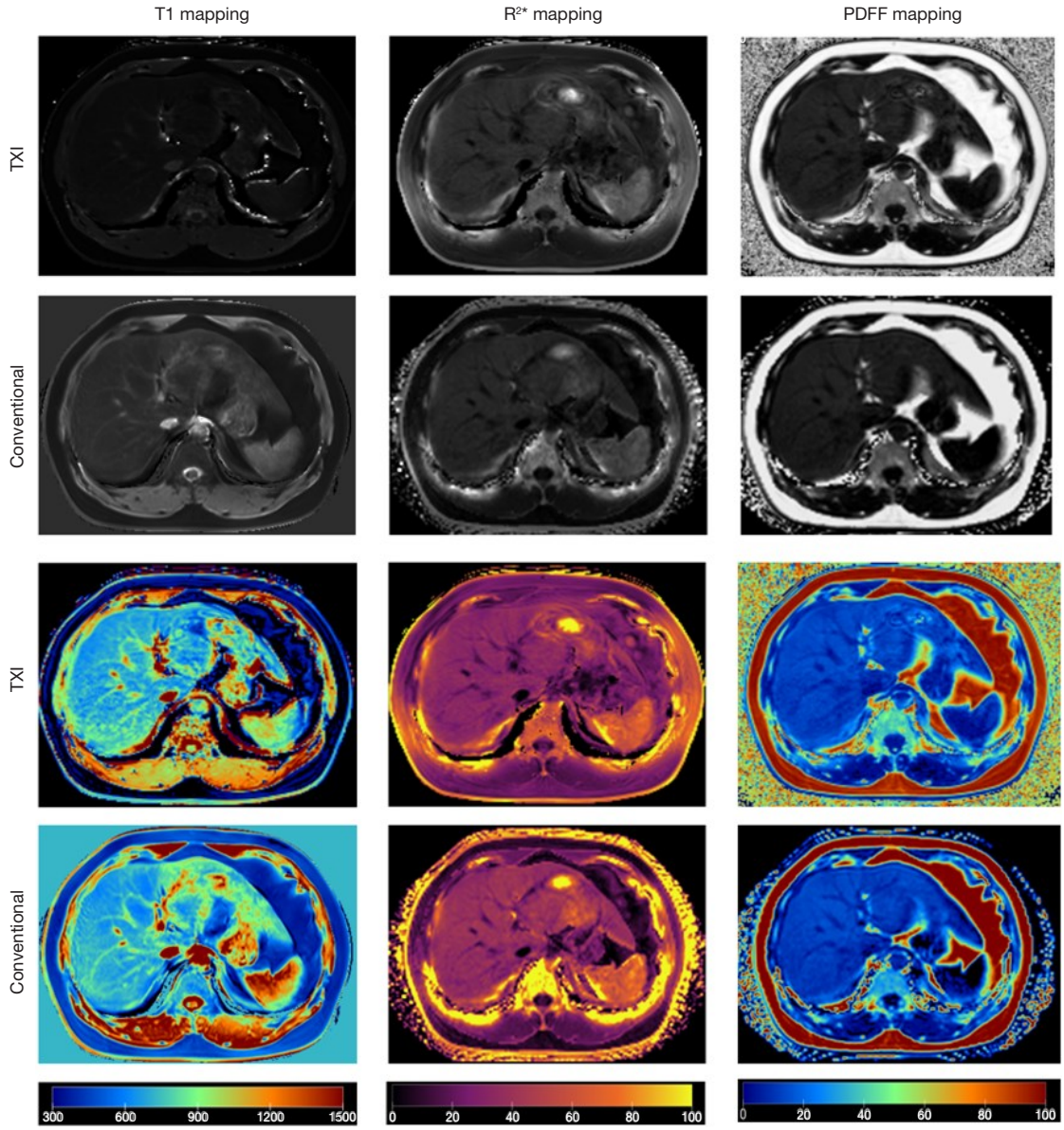

Figure 6 Original images of TXI and conventional MRI sequences (top two rows) are presented alongside their corresponding false color representations (bottom two rows) for a 56-year-old NAFLD patient. The mean T1, R2*, and PDFF values measured by TXI were 859 ms, 60 s^{-1}, and 10.9%, respectively. The mean T1, R2*, and PDFF values measured by reference quantitative MRI were 852 ms, 60 s^{-1}, and 10.6%, respectively. MRI, magnetic resonance imaging; NAFLD, non-alcoholic fatty liver disease; PDFF, proton density fat fraction; TXI, multi-relaxation-time imaging.

invasive method for characterizing liver tissue. It provides comprehensive qualitative and quantitative information, including T1, R2*, and PDFF maps, which were highly consistent with reference quantitative values. This suggests that the method has the potential to serve as a biomarker for fibrosis, liver fat, and liver iron overload simultaneously. Its ability to obtain liver quantitative parameters in only 19 seconds highlights its potential significance in the diagnosis and treatment of liver diseases. Future research should include a larger sample size of liver disease patients and biopsy samples to further evaluate the role of TXI technology in the detection and treatment of liver diseases.

Acknowledgments

None.

Footnote

Reporting Checklist: The authors have completed the STROBE reporting checklist. Available at https://qims.amegroups.com/article/view/10.21037/qims-24-1786/rc

Funding: The study was supported by the Key Research and Development Project of Sichuan Province Science and Technology Department (No. 2023YFS0227) and the Research Project of Sichuan Provincial Cadre Health (No. 2023-215).

Conflicts of Interest: All authors have completed the ICMJE uniform disclosure form (available at https://qims.amegroups.com/article/view/10.21037/qims-24-1786/coif). M.C. is an employee of Siemens Healthineers. The other authors have no conflicts of interest to declare.

Ethical Statement: The authors are accountable for all aspects of the work in ensuring that questions related to the accuracy or integrity of any part of the work are appropriately investigated and resolved. The study was conducted in accordance with the Declaration of Helsinki and its subsequent amendments. The study was approved by the Institutional Review Board of Sichuan Academy of Medical Sciences & Sichuan Provincial People's Hospital, University of Electronic Science and Technology of China (No. 2023-550), and written informed consent was obtained from all participants before MRI.

References

1. Riazi K, Azhari H, Charette JH, Underwood FE, King JA, Afshar EE, Swain MG, Congly SE, Kaplan GG, Shaheen AA. The prevalence and incidence of NAFLD worldwide: a systematic review and meta-analysis. Lancet Gastroenterol Hepatol 2022;7:851-61.
2. Powell EE, Wong VW, Rinella M. Non-alcoholic fatty liver disease. Lancet 2021;397:2212-24.
3. Lee YA, Wallace MC, Friedman SL. Pathobiology of liver fibrosis: a translational success story. Gut 2015;64:830-41.
4. Starley BQ, Calcagno CJ, Harrison SA. Nonalcoholic fatty liver disease and hepatocellular carcinoma: a weighty connection. Hepatology 2010;51:1820-32.
5. Rockey DC, Caldwell SH, Goodman ZD, Nelson RC, Smith AD; . Liver biopsy. Hepatology 2009;49:1017-44.
6. Ratziu V, Charlotte F, Heurtier A, Gombert S, Giral P, Bruckert E, Grimaldi A, Capron F, Poynard T; . Sampling variability of liver biopsy in nonalcoholic fatty liver disease. Gastroenterology 2005;128:1898-906.
7. Banerjee R, Pavlides M, Tunnicliffe EM, Piechnik SK, Sarania N, Philips R, Collier JD, Booth JC, Schneider JE, Wang LM, Delaney DW, Fleming KA, Robson MD, Barnes E, Neubauer S. Multiparametric magnetic resonance for the non-invasive diagnosis of liver disease. J Hepatol 2014;60:69-77.
8. Venkatesh SK, Yin M, Ehman RL. Magnetic resonance elastography of liver: technique, analysis, and clinical applications. J Magn Reson Imaging 2013;37:544-55.
9. Li Z, Sun J, Hu X, Huang N, Han G, Chen L, Zhou Y, Bai W, Yang X. Assessment of liver fibrosis by variable flip angle T1 mapping at 3.0T. J Magn Reson Imaging 2016;43:698-703.
10. Luetkens JA, Klein S, Träber F, Schmeel FC, Sprinkart AM, Kuetting DLR, Block W, Uschner FE, Schierwagen R, Hittatiya K, Kristiansen G, Gieseke J, Schild HH, Trebicka J, Kukuk GM. Quantification of Liver Fibrosis at T1 and T2 Mapping with Extracellular Volume Fraction MRI: Preclinical Results. Radiology 2018;288:748-54.
11. Erden A, Kuru Öz D, Peker E, Kul M, Özalp Ateş FS, Erden İ, İdilman R. MRI quantification techniques in fatty liver: the diagnostic performance of hepatic T1, T2, and stiffness measurements in relation to the proton density fat fraction. Diagn Interv Radiol 2021;27:7-14.
12. Zou J, Jiang Y, Fan F, Yang P, Gan T, Yang T, Li M, Ding Y, Wang S, Zhang J. The application of B1 inhomogeneity-corrected variable flip angle T1 mapping for assessing liver fibrosis. Magn Reson Imaging 2024;113:110215.
13. Hankins JS, McCarville MB, Loeffler RB, Smeltzer MP, Onciu M, Hoffer FA, Li CS, Wang WC, Ware RE, Hillenbrand CM. R2* magnetic resonance imaging of the liver in patients with iron overload. Blood

2009;113:4853-5.
14. Wood JC, Zhang P, Rienhoff H, Abi-Saab W, Neufeld EJ. Liver MRI is more precise than liver biopsy for assessing total body iron balance: a comparison of MRI relaxometry with simulated liver biopsy results. Magn Reson Imaging 2015;33:761-7.
15. d'Assignies G, Paisant A, Bardou-Jacquet E, Boulic A, Bannier E, Lainé F, Ropert M, Morcet J, Saint-Jalmes H, Gandon Y. Non-invasive measurement of liver iron concentration using 3-Tesla magnetic resonance imaging: validation against biopsy. Eur Radiol 2018;28:2022-30.
16. Qi Q, Weinstock AK, Chupetlovska K, Borhani AA, Jorgensen DR, Furlan A, Behari J, Molinari M, Ganesh S, Humar A, Duarte-Rojo A. Magnetic resonance imaging-derived proton density fat fraction (MRI-PDFF) is a viable alternative to liver biopsy for steatosis quantification in living liver donor transplantation. Clin Transplant 2021;35:e14339.
17. Park CC, Nguyen P, Hernandez C, Bettencourt R, Ramirez K, Fortney L, Hooker J, Sy E, Savides MT, Alquiraish MH, Valasek MA, Rizo E, Richards L, Brenner D, Sirlin CB, Loomba R. Magnetic Resonance Elastography vs Transient Elastography in Detection of Fibrosis and Noninvasive Measurement of Steatosis in Patients With Biopsy-Proven Nonalcoholic Fatty Liver Disease. Gastroenterology 2017;152:598-607.e2.
18. Noureddin M, Lam J, Peterson MR, Middleton M, Hamilton G, Le TA, Bettencourt R, Changchien C, Brenner DA, Sirlin C, Loomba R. Utility of magnetic resonance imaging versus histology for quantifying changes in liver fat in nonalcoholic fatty liver disease trials. Hepatology 2013;58:1930-40.
19. Tang A, Tan J, Sun M, Hamilton G, Bydder M, Wolfson T, Gamst AC, Middleton M, Brunt EM, Loomba R, Lavine JE, Schwimmer JB, Sirlin CB. Nonalcoholic fatty liver disease: MR imaging of liver proton density fat fraction to assess hepatic steatosis. Radiology 2013;267:422-31.
20. Ahn JH, Yu JS, Park KS, Kang SH, Huh JH, Chang JS, Lee JH, Kim MY, Nickel MD, Kannengiesser S, Kim JY, Koh SB. Effect of hepatic steatosis on native T1 mapping of 3T magnetic resonance imaging in the assessment of T1 values for patients with non-alcoholic fatty liver disease. Magn Reson Imaging 2021;80:1-8.
21. Li S, Wang Z, Ding Z, She H, Du YP. Accelerated four-dimensional free-breathing whole-liver water-fat magnetic resonance imaging with deep dictionary learning and chemical shift modeling. Quant Imaging Med Surg 2024;14:2884-903.
22. Wang Y, Qi H, Wang Y, Xiao M, Xiang C, Dong J, Chen H. Free-breathing simultaneous water-fat separation and T1 mapping of the whole liver (SWALI) with isotropic resolution using 3D golden-angle radial trajectory. Quant Imaging Med Surg 2023;13:912-23.
23. Wang N, Cao T, Han F, Xie Y, Zhong X, Ma S, Kwan A, Fan Z, Han H, Bi X, Noureddin M, Deshpande V, Christodoulou AG, Li D. Free-breathing multitasking multi-echo MRI for whole-liver water-specific T1 , proton density fat fraction, and R2* quantification. Magn Reson Med 2022;87:120-37.
24. Wang YS, Huang T, Chen ML, Yan X, Yin LY. Comparison of R1, R2* and the PDFF mapping by simultaneous multi-relaxation-time Imaging (TXI) method in hepatic disease. Proceedings of the 23st Annual Meeting of ISMRM, Toronto, ON, Canada, 2023. Available online: https://archive.ismrm.org/2023/5190.html
25. Yang J, Liu Y, Hang W, Chen M, Li J, Yi Y, Zhong H, Yan X. Feasibility study of a simultaneous multi-relaxation-time Imaging (TXI) method in Intervertebral Disc. Proceedings of the 23st Annual Meeting of ISMRM, Toronto, ON, Canada, 2023. Available online: https://archive.ismrm.org/2023/4957.html
26. Ren J, Dimitrov I, Sherry AD, Malloy CR. Composition of adipose tissue and marrow fat in humans by 1H NMR at 7 Tesla. J Lipid Res 2008;49:2055-62.
27. Hamilton G, Yokoo T, Bydder M, Cruite I, Schroeder ME, Sirlin CB, Middleton MS. In vivo characterization of the liver fat ^{1}H MR spectrum. NMR Biomed 2011;24:784-90.
28. Hernando D, Levin YS, Sirlin CB, Reeder SB. Quantification of liver iron with MRI: state of the art and remaining challenges. J Magn Reson Imaging 2014;40:1003-21.
29. Fram EK, Herfkens RJ, Johnson GA, Glover GH, Karis JP, Shimakawa A, Perkins TG, Pelc NJ. Rapid calculation of T1 using variable flip angle gradient refocused imaging. Magn Reson Imaging 1987;5:201-8.
30. Akoglu H. User's guide to correlation coefficients. Turk J Emerg Med 2018;18:91-3.
31. European Association for the Study of the Liver (EASL); European Association for the Study of Diabetes (EASD); European Association for the Study of Obesity (EASO). EASL-EASD-EASO Clinical Practice Guidelines for the management of non-alcoholic fatty liver disease. J Hepatol 2016;64:1388-402.
32. Tadimalla S, Wilson DJ, Shelley D, Bainbridge G, Saysell M, Mendichovszky IA, Graves MJ, Guthrie JA, Waterton JC, Parker GJM, Sourbron SP. Bias, Repeatability and

Reproducibility of Liver T(1) Mapping With Variable Flip Angles. J Magn Reson Imaging 2022;56:1042-52.
33. Ghavamian A, Liu C, Kang B, Yuan X, Wang X, Gao L, Zhao X. Liver T1 relaxation time of the 'normal liver' in healthy Asians: measurement with MOLLI and B1-corrected VFA methods at 3T. Br J Radiol 2022;95:20211008.
34. Hui SCN, So HK, Chan DFY, Wong SKH, Yeung DKW, Ng EKW, Chu WCW. Validation of water-fat MRI and proton MRS in assessment of hepatic fat and the heterogeneous distribution of hepatic fat and iron in subjects with non-alcoholic fatty liver disease. Eur J Radiol 2018;107:7-13.
35. Reeder SB, Pineda AR, Wen Z, Shimakawa A, Yu H, Brittain JH, Gold GE, Beaulieu CH, Pelc NJ. Iterative decomposition of water and fat with echo asymmetry and least-squares estimation (IDEAL): application with fast spin-echo imaging. Magn Reson Med 2005;54:636-44.
36. Yu H, McKenzie CA, Shimakawa A, Vu AT, Brau AC, Beatty PJ, Pineda AR, Brittain JH, Reeder SB. Multiecho reconstruction for simultaneous water-fat decomposition and T2* estimation. J Magn Reson Imaging 2007;26:1153-61.
37. Hernando D, Kramer JH, Reeder SB. Multipeak fat-corrected complex R2* relaxometry: theory, optimization, and clinical validation. Magn Reson Med 2013;70:1319-31.
38. Yu H, Shimakawa A, Hines CD, McKenzie CA, Hamilton G, Sirlin CB, Brittain JH, Reeder SB. Combination of complex-based and magnitude-based multiecho water-fat separation for accurate quantification of fat-fraction. Magn Reson Med 2011;66:199-206.
39. Messroghli DR, Radjenovic A, Kozerke S, Higgins DM, Sivananthan MU, Ridgway JP. Modified Look-Locker inversion recovery (MOLLI) for high-resolution T1 mapping of the heart. Magn Reson Med 2004;52:141-6.
40. Sengupta A, Gupta RK, Singh A. Evaluation of B(1) inhomogeneity effect on DCE-MRI data analysis of brain tumor patients at 3T. J Transl Med 2017;15:242.
41. Treier R, Steingoetter A, Fried M, Schwizer W, Boesiger P. Optimized and combined T1 and B1 mapping technique for fast and accurate T1 quantification in contrast-enhanced abdominal MRI. Magn Reson Med 2007;57:568-76.

Cite this article as: Jiang Y, Yin P, Wang Y, Chen M, Yin L. Rapid liver tissue characterization using simultaneous multi-relaxation-time imaging: a comparative study with conventional magnetic resonance imaging. Quant Imaging Med Surg 2025;15(5):4400-4413. doi: 10.21037/qims-24-1786